Royal Netherlands
Meteorological Institute
Ministry of Infrastructure and the Environment

Storm surges and high discharge

A joint probabilities study

Sarah Kew, Frank Selten and Geert Lenderink

De Bilt, 2011 | Scientific report; WR 2011-05

Storm surges and high discharge

Version 1.0

Date December 30, 2011
Status FINAL

Colofon

Title	Storm surges and high discharge *A joint probabilities study*
Authors	S.F. Kew G. Lenderink F.M. Selten
Contact	sarah.kew@knmi.nl KNMI | Global Climate Wilhelminalaan 10 | 3732 GK De Bilt Postbus 201 | 3730 AE De Bilt

Knowledge for Climate

Table of contents

Summary

The low-lying Netherlands is at risk from multiple threats of sea level rise, storm surges and extreme river discharges. Should these threats occur simultaneously, a catastrophe will be at hand. Knowledge about the likelihood of simultaneous occurance or the so-called 'joint probability' of such threats is essential to provide guidance on legislation for dike heights, flood barrier design and water management in general.

In this study, we explore the simultaneous threats of North Sea storm surges and extreme Rhine river discharge for the current climate in a large 17-member global climate model ensemble. We use a simple approach, taking proxies of North-Northwesterly winds over the North Sea and multiple-day precipitation averaged over the Rhine for storm surge and discharge respectively, so that a sensitivity analysis is straight forward to apply. By investigating soft extremes, we circumvent the need to extrapolate the data and thereby permit the synoptic development of selected events to be inspected.

Our principle finding is that the probability of extreme surge conditions following extreme 20-day precipitation sums is around 3 times higher than that estimated from treating extreme surge and discharge probabilities as independent, as previously assumed.

1 Introduction

1.1 Storm surge barrier closure

The storm surge barrier near Hoek van Holland closes automatically when the water level is predicted to exceed the mean sea level by more than 3m (Van den Brink et al., 2005). The water level depends on both sea conditions (tide and surge) and the Rhine river discharge. The decision of if and when to close the barrier might be complicated in the case of a simultaneous extreme surge and extreme discharge event. In the event of an extreme discharge alone, the barrier should remain open to prevent the damming of excess water. In the event of a surge, the barrier should be closed to protect the densely populated Rotterdam area.

1.2 Reported related research

There has been a limited amount of research into the joint probability of storm surges and high Rhine discharge. Currently the probabilities of the two events are treated independently, assuming that the correlation between them is small, but the issue of independence is still under debate.

The study by Van den Brink et al. (2005), featuring a short assessment on storm surge barrier closure, finds no apparent positive correlation between the amplitude of North Sea surges and Rhine discharges. Most barrier-closure conditions in their data were caused by a high surge level and were relatively insensitive to extreme river discharge. They concentrated on 20-day precipitation sums accumulated over the Rhine basin and modelled the discharge at Lobith using an empirically tuned simple water balance equation, accounting for large-scale and convective precipitation, evaporation and snow accumulation (Van den Brink et al., 2005, equation 4). The input fields were taken from ECMWF seasonal forecast ensembles (1987-2004) amounting to 1570 years of data. The high tide surge was calculated following equation 1 of Van den Brink et al. (2004) using the 12-hour averaged wind speed and direction at a central grid box over the North Sea and the sea level pressure (SLP) (for the barometric pressure effect) at Hoek van Holland.

Mentioned limitations of the Van den Brink et al. (2005) study are (1) the period 1987-2004 might not be entirely representative of the full range of the present climate, (2) the simple downscaling relations used for the surge height and discharge might be better replaced by advanced models — the water-level return periods calculated from the ensemble forecasts are slightly shorter than those observed, although might still be considered the same within the margins of error. We add some further thoughts below.

Their conclusion that there is no positive correlation between the amplitude of North Sea surges and Rhine discharges is drawn from their Fig. 6b (Van den Brink et al., 2005), reproduced here in our Fig. 1.1, which displays a scatter plot of the water level at Hoek van Holland versus the Rhine discharge at Lobith. We note from the same figure, however, that the spread of sea levels does show some dependency on discharge. For example, the lowest sea levels are obtained only when the discharge is also low, and high discharges (limited data) occur only with medium-range sea-levels. The relationship between the extreme discharges and surges could be investigated more thoroughly. An examination of the synoptic situation for the extreme events would also give insight beyond correlation statistics into the physical evolution of the scenario and thus if and how a joint extreme event (simultaneous high discharge and storm surge) might occur.

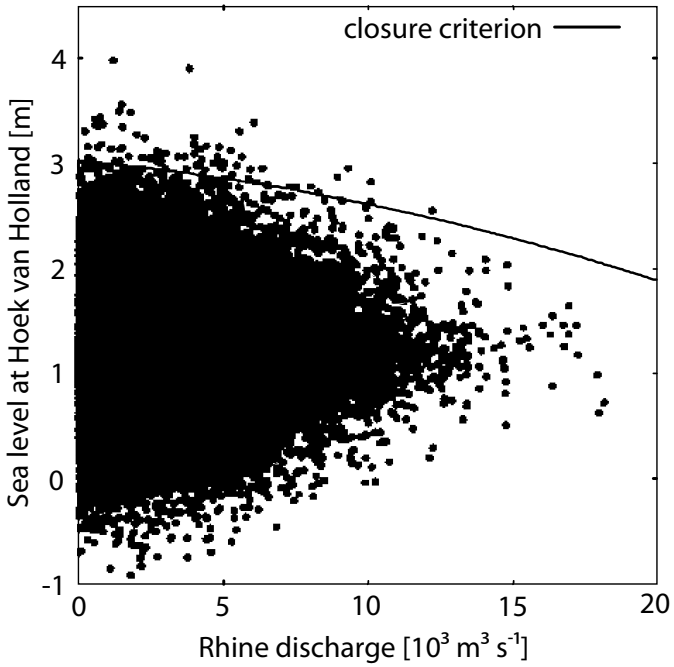

Figure 1.1: A reproduction of Fig. 6b from Van den Brink et al. (2005). Scatter plot of the water level at Hoek van Holland versus the Rhine discharge for all high-tide values of the water level at Rotterdam, together with the closure criterion of 3m. Values are calculated from the ECMWF global seasonal forecast data set. According to their analysis, the closure criterion is exceeded once every 8.1 years.

1.2.1 Surge-favourable meteorological situation

The Dutch coast is at risk from storm surges when strong North or Northwesterly (Sterl et al., 2009) winds are present over the North Sea, as these wind directions have the largest fetch. The meteorological situation leading to these conditions and present in the highest observed (Van den Brink et al., 2004) and modelled (Van den Brink et al., 2004; Sterl et al., 2009) surges is a large-scale depression centred over or near southern Scandinavia (see Fig. 1.2).

It is conceivable that the synoptic system responsible for the surge-favourable conditions may also be responsible for or contribute to heavy precipitation over the Rhine basin, associated with fronts extending downstream and south of the large-scale system. Alternatively, when the large-scale mid-tropospheric flow is westerly, known as a west wind 'Wetterlage', a series of depressions associated with waves on the polar front move across the Atlantic towards central Europe. Typically the depressions are separated by one to two days and the westerly flow conditions last on the order of a week. In this flow configuration, precipitation may accumulate in the Rhine basin from one or more systems passing in short succession, with northerly winds most likely to follow behind each system.

1.2.2 Effect of a warming climate

This document focusses on the current climate. Nevertheless, we include a brief section on the effect of a warming climate. Sterl et al. (2009) conducted a study of extreme North Sea surges by forcing a surge model with meteorological input from a 17-member ensemble of the ECHAM-05/MPI global climate model. They calculated 10 000-yr return surge levels and found no statistically significant change for the

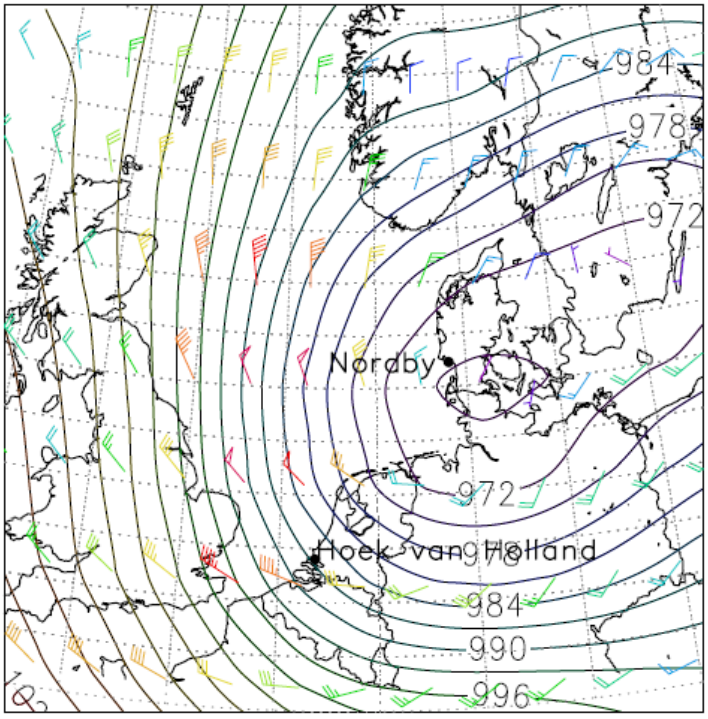

Figure 1.2: The sea level pressure and surface winds for the most severe surge conditions at Hoek van Holland, simulated in the ESSENCE-forced surge model WAQUA/DCSM98 — a reproduction of Fig. 2b from Sterl et al. (2009).

Dutch coast during the 21st century. Some climate modelling studies suggest there will be an increase in the frequency of westerly winds but there is no support for a change towards more Northerly (surge-favouring) winds. The contribution from high river discharge is not taken into account. Multiday precipitation extremes, however, are likely to increase in intensity (winter) (Kew et al., 2011). The combined probability of a storm surge and high discharge could therefore also change for a warmer climate. In addition, the number of barrier-closures is expected to increase (exponentially) with sea-level rise and the duration of closure will also increase (Van den Brink et al., 2005; Katsman et al., 2011).

1.2.3 *Idealised approach*

There are multiple factors affecting both discharge and wave height, such as land use and tides. Rather than using discharge and surge models to encompass all complexities, we instead (as a starting point) take a more idealised approach, using simple parameters as proxies for high discharge and storm surge, calculated using a large global climate model ensemble. We study the effect of small changes to these parameters on the probability of a joint-event in order to gain some understanding of the sensitivity of the results to the choices made.

Our results will offer answers to two basic questions:

1. After extreme precipitation over the Rhine basin, what is the probability distribution of North Sea wind strength and direction compared with climatology?
2. Is there an enhanced probability of a storm surge after a period of extreme precipitation over the Rhine basin?

2 Methods

2.1 Data set

All data used are derived from the ESSENCE data set (Sterl et al., 2008) – a 17-member ensemble simulation spanning the years 1950–2100, generated from the ECHAM5/MPI-OM coupled global climate model. It has a horizontal resolution of T63 and 31 vertical hybrid atmospheric levels, and is forced by the SRES A1b scenario (Nakićenović et al., 2000). The different ensemble members are formed by perturbing the initial state of the atmosphere, with ocean conditions unchanged.

We only make use of the early years, 1950–1980, representing the current climate and the winter season DJF. All wind variables are derived from daily averages of 10 m zonal and meridional wind components. Other variables extracted are daily precipitation, and mean sea level pressure.

2.2 Discharge and surge definitions and study region

We make the following choices to identify extreme discharges and storm surges in the data set. We assume that a high discharge occurs if the quantile q_x^r of n-day basin-averaged precipitation sums, r_n (where x is fixed at 99% and n takes a value in the range of 1-20 days), is exceeded. The set of precipitation events meeting the condition $r_n > q_{0.99}^r$ is marked with an asterisk, r_n^*.

We assume that an imminent storm surge is expected when the daily average NNW wind component w_1 (extracted over a suitable domain in the North Sea) exceeds the distribution's quantile q_x^w. Here x is also chosen to be 99%. The set of wind events meeting the condition $w_1 > q_{0.99}^w$ is marked with an asterisk, w_1^*.

If extreme discharge events and storm surges occur independently, we can expect the probability of observing a surge $P(w_1^*)$ to be fixed at $1 - x = 0.01$ regardless of (any extremes in) the precipitation history, i.e. $P(w_1^*|r_n^*) = 0.01$.

Note that the 99% quantile is a soft extreme, approximately equivalent to a return period of 1 year. We choose soft extremes in order to ensure that a reasonably sized sample of joint events is available in the data set (see next section for the expected sample size). Statistical methods can be used to estimate the return periods of extremes beyond those observed in the data, far into the tails of the individual event distributions. Modelling extremes of the *joint* events would be more challenging. However, we also wish to examine the synoptic (physical) evolution in the lead up to the extreme joint events, for which we require the events to be observed in the data series, as opposed to being modelled from it. In this preliminary study we therefore investigate soft extremes alone.

Figure 2.1 illustrates the regions taken to be relevant for this investigation. The Rhine basin is represented by a box of 12-grid cells, centred over Germany. Wind conditions are assessed within a box over the North Sea. The boundaries of the North Sea box were chosen based on the region of strong winds shown in the synoptic map for the strongest surge in ESSENCE found by Sterl et al. (2009) (their Fig. 2b, here reproduced in Fig. 1.2).

2.3 Assessing joint-probability and sampling error

For a 30-year period, a 90-day DJF season and 17 ensemble members, ESSENCE provides $30 \times 90 \times 17 = 45900$ events. Note that we do not restrict the analysis to

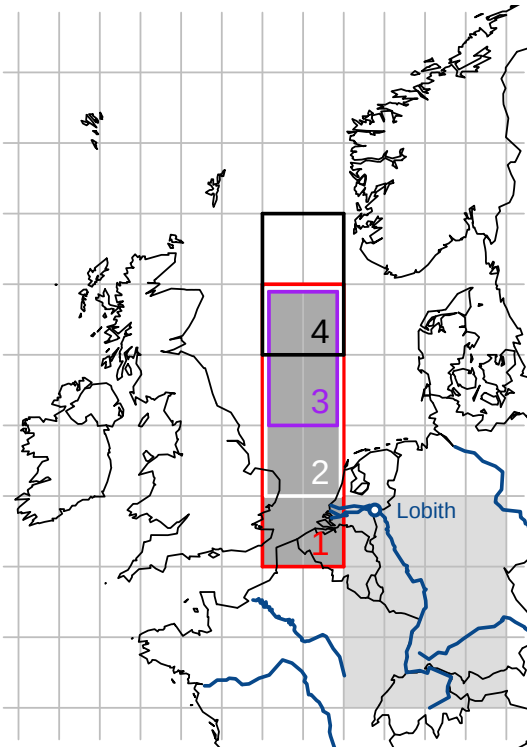

Figure 2.1: ESSENCE grid cells (grey grid) selected to represent the rhine basin (light grey shading) and assess the wind conditions favorable for surges (dark grey shading). Numbered boxes indicate the configurations used for sensitivity testing in Sec. 3.5.

independent (non-overlapping) events. Therefore, 459 events will exceed the $q^r_{0.99}$ threshold by construction. If the probability of a storm surge is independent of precipitation history, we can expect on the order of 4–5 joint (high discharge and surge) events to occur by chance. If the events are not independent, we should see a significantly larger number of joint events, or a smaller number in the case of an inhibiting effect. We express the magnitude of change in the joint probability by a scale factor, S, obtained by normalising the result by the expected independent probability $P(r^*_n) \equiv 0.01$:

$$S_{joint} = \frac{P(w^*_1|r^*_n)}{P(r^*_n)} \tag{2.1}$$

Naturally there will be some sampling error associated with the number of joint events that actually occur or the number that are expected to occur by chance. To obtain an estimate of the amplitude of sampling error, we take 1000 random samples of the same size (459) as the precipitation-conditioned sample. From these samples, we obtain a range of PDFs for the wind direction, speed and NNW component. In this case, the exceedance of the climatological $q_{0.99}$ thresholds is given by

$$\widetilde{S}_{joint} = \frac{P(w^*_1|\widetilde{r}_n)}{P(r^*_n)}, \tag{2.2}$$

where the tilde denotes a quantity derived from a random sample.

We present figures for the distribution of exceedances (2) compared to the precipitation-conditioned sample (1). We also show the wind PDFs (not restricting to wind extremes) and their anomaly to the climatological PDFs for both the precipitation conditioned sample, $P(w_1|r_{n*})$, and the random samples, $P(w_1|\widetilde{r}_n)$.

2.4 Projection onto (surge) NNW axis

The NNW unit vector is denoted $\mathrm{s} = \cos\theta\hat{\mathrm{i}} + \sin\theta\hat{\mathrm{j}}$ where $\theta = -67.5^\circ$ is the angle measured anticlockwise from the horizontal axis (convention in vector calculus) and $\hat{\mathrm{i}}$ and $\hat{\mathrm{j}}$ are unit vectors in the zonal and meridional directions.
The projection of the wind vector, $\mathrm{v} = u\hat{\mathrm{i}} + v\hat{\mathrm{j}}$, onto the NNW axis is given by $\mathrm{v}\cdot\mathrm{s} = u\cos(67.5^\circ)\hat{\mathrm{i}} - v\sin(67.5^\circ)\hat{\mathrm{j}}$.

The projected wind field is averaged over the North Sea box with equal weighting for each grid cell.

2.5 Area-average wind direction

The resultant unit wind vector for a box of *N* grid cells is found from

$$\hat{\mathrm{w}} = \frac{\sum_{k=1}^{N}\hat{\mathrm{v}}_\mathrm{k}}{\|\sum_{k=1}^{N}\hat{\mathrm{v}}_\mathrm{k}\|} \tag{2.3}$$

where $\hat{\mathrm{v}}_\mathrm{k}$ is the unit vector in the direction of the wind in a single grid cell *k*. The compass bearing, ϕ, (angle from which the wind is coming, measured clockwise from North following meteorological convention) is given by the inverse tangent of the ratio of the zonal to meridional component of the resultant wind vector. This can be written as

$$\phi = \tan^{-1}\left(\frac{\sum_{k=1}^{N} u_k/\|\mathrm{v}_k\|}{\sum_{k=1}^{N} v_k/\|\mathrm{v}_k\|}\right) + 180^\circ \tag{2.4}$$

This measure is used to present only the unconditional probability density function for the North Sea wind climatology.

2.6 Variable parameters

The number of joint events identified in the data set and, consequently, our estimate of the joint event probability could be sensitive to our choice of parameters defining the surge and discharge proxies. In this document we will look at the sensitivity of the results to the configuration of the North Sea wind assessment box and the precipitation interval, *n*.

The default set-up for the reference date in the *n*-day precipitation block and the timing of the wind assessment is illustrated in Fig. 2.2. It is also possible in our scheme to set a lag between the wind assessment and the peak of the weighted precipitation maximum (a centre of mass calculation) within a block. In the current study, we simply use the default set-up with zero lag.

There are several other variable parameters which may be varied in the set-up we have used. These will be mentioned in the final section.

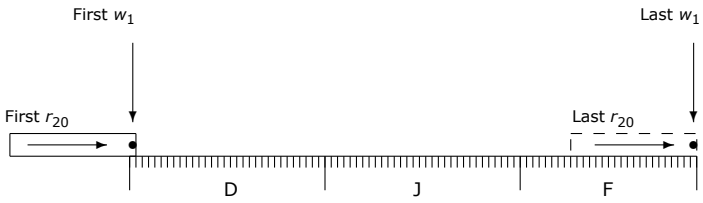

Figure 2.2: Illustration of relative phasing for the series of 20-day precipitation sums, r_{20}, and daily wind, w_1, during the DJF season. A total of 90 n-day precipitation sums are created each ending *on a subsequent day of the DJF season. Short vertical lines separate individual days. Long vertical lines separate months. Point markers indicate the* reference *day for each precipitation block. The lag between the precipitation reference day and the wind record is fixed, in this case to 0 days.*

3 Results

3.1 Climatology of North Sea winds

In Fig. 3.1 the DJF climatologies (1950–1980) of North Sea box-mean wind direction, wind speed and NNW wind components are presented. It is seen in (a) that the most common wind direction is SW, and a NNW direction (right-most bin) occurs with just over one third of the peak frequency. The peak frequency in NNW wind component (c) is slightly negative, which is consistent with (a) as the SW direction projects negatively onto the NNW axis. The $q^{w}_{0.99}$ threshold is 12.0 ms^{-1} in the NNW direction.

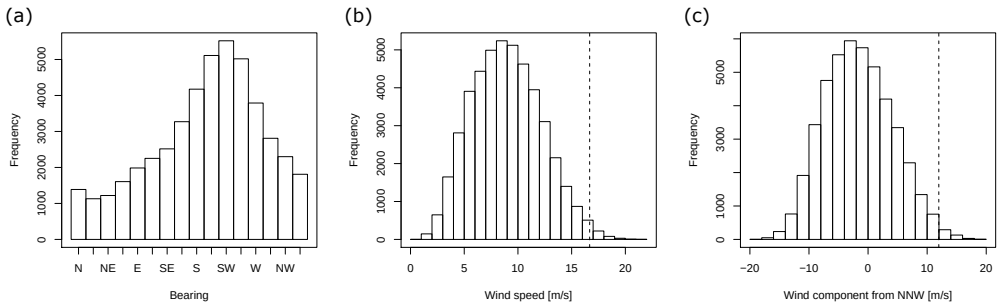

Figure 3.1: DJF Climatology (1950–1980) of wind directions (a), wind speed (b) and NNW wind component (c) averaged over the North Sea box (shaded dark grey in Fig. 2.1). The dashed vertical line in (b) and (c) marks the location of the 99% quantiles.

3.2 Wind direction conditioned on heavy precipitation

Fig. 3.2 shows the PDF of North Sea wind direction following heavy precipitation over the Rhine basin and, on the right side, the PDF's anomaly with respect to the full climatology of Fig. 3.1a. The 95% range in frequency density obtained from the PDFs of 1000 random samples of the total population (described in Section 2.3) are presented as a shaded region to illustrate the magnitude of error due to sample size.

A significant departure from the climatological PDF (climatology effectively represented by the shaded band) is evident. For 1-day precipitation events (top row), the peak of the wind direction distribution has rotated clockwise with respect to climatology, favouring westerlies, whilst the NNW direction is not favoured more than in the climatology. For 2-day extremes (not shown) the peak rotates further towards the North. For 5-day events (second row), the North-West quarter is favoured significantly and southerlies are suppressed. For 20-day sums (lower row), the distribution of wind directions is relaxing towards the climatology.

A summary of the anomalous probability density (data identical to the bars in the right-hand panels of Fig. 3.2) for all n-day sums considered is displayed in Fig. 3.3. With this representation, the pattern of clockwise rotation of the peak of the distribution as n increases can be made out, as a diagonal of positive anomalies. An explanation is that, as n increases, the timing of the passage of the precipitating system or front within the n-day period is less restricted. A separation in time between the heaviest precipitation and the assessment of the wind criterion becomes possible and effectively the system has time to pass, leaving Northerly winds in its wake. The strongest positive departure from climatology is found for n = 2, but positive anomalies in the NW quarter are still present even following 20-day precipitation extremes.

3.3 Wind speed conditioned on heavy precipitation

Fig. 3.4 shows the PDFs of North Sea wind speed following heavy precipitation over the Rhine basin. For 1-day precipitation events (top row), there is a shift of the PDF towards higher wind speeds. The anomaly to the climatology (Fig. 3.4(b)) clearly extends beyond the limits of sampling error. For larger n however (row 2 and 3), the conditional distribution is close to the climatology. The summary diagram, Fig. 3.5, indicates coherency in the anomaly sign only for precipitation events of length $n = 1$ and $n = 2$. For longer precipitation sums, there is no strongly significant shift of the North Sea wind speed probability density function.

To quantify the changes to the extreme end of the distribution, we display the proportion of the conditional sample (triangle marker) as well as of each random sample (histogram) that exceeds the $q_{0.99}$ threshold for wind speed (Fig. 3.6) and thus classed as extreme. The conditional sample exceedance is an estimate of the true joint probability, $P(w_1^*|r_n^*)$ that is limited by the sample size. We expect the random sample exceedances to be distributed about the climatological exceedance, which is 0.01 by construction, with a spread associated with the error due to sample size. When the conditional sample exceedance lies outside of the 99% range of random sample exceedances, we assume that the probability of the joint event is significantly different to climatology.

The exceedance is significant for $n = 1$ (Fig. 3.6a). For $n = 5$ (Fig. 3.6b) and $n = 20$ (Fig. 3.6c), there is an indication that slightly higher exceedances than normal can be expected, but the departure from climatology is not significant.

3.4 NNW wind component conditioned on heavy precipitation

Fig. 3.7 shows the PDFs of the magnitude of the NNW wind component over the North Sea, following heavy precipitation over the Rhine basin. A shift of the PDF to larger positive magnitudes is apparent for all n-day sums considered. The change is significant for magnitudes exceeding $q^w_{0.99}$. The summary of the probability density anomaly in Fig. 3.8 shows coherency in the anomaly sign over all $n-$day precipitation sums. The exceedances of the $q^w_{0.99}$ threshold are significant for all n-day precipitation accumulation periods considered (Fig. 3.9). For example, extreme NNW winds (red triangle) are 3-4 times more likely (than the climatological probability of 1%) following 20-day extreme rainfall events over the Rhine basin (Fig. 3.9c).

3.5 Sensitivity to the assessment location for wind conditions

Figure 3.10a shows the impact on the estimated scaled joint probability, S_{joint} (eq. 1), of changing the size and position of the North Sea box used to assess the NNW wind component. Box 1 (red contour in Fig. 2.1) and Box 2 (white contour, top three rows of Box 1) give similar results for all n-day sums. Box 1 and 2 are more elongated than Box 3 (purple contour, top two rows of Box 1) and 4 (black contour, Box 3 shifted one row further North). The assessment of NNW conditions in a large or elongated box may favour the selection of larger synoptic systems. Larger spatial and temporal correlations might then be expected, favouring larger joint probabilities of events over the Rhine Basin and the North Sea.

Van den Brink et al. (2004) use model wind data from a single location over the North Sea to model surges. The location corresponds closest to the North-East most cell of Box 1, thus their wind input, and potentially their results, should be most similar to those attained from Box 3 or 4.

The largest joint probabilities attained for all boxes are found following 2-day precipitation events and probably signifies that the same synoptic system is

responsible for heavy rain and the subsequent surge created by the increase in Northerly winds as the system passes (Fig. 3.10a). A second peak in joint probability occurs at 10 days for Box 1, 2 and 3. This probably signifies that the precipitation is generated from more than one synoptic system – the first of which does not necessarily contribute to the surge conditions, and 10 days is more than enough for the full passage of at least 2 depressions.

The joint probabilities are raised up to a factor of 5 above the unconditional probability of a surge, following a 2-day precipitation extreme. For a 10-day precipitation extreme, S_{joint} ranges from about 2 to 4.3, depending on the region used for wind assessment. For a 20-day precipitation extreme, S_{joint} ranges between about 1.3 to 3.3.

3.6 Composites

In Fig. 3.11 we present SLP climatologies for the DJF season. The full season climatology (a) shows a region of low pressure extends across the Atlantic between Greenland and the UK – the storm track. The climatology of days satisfying the NNW extreme wind condition (b) shows a low pressure centre over Southern Scandinavia and a ridge North of the Azores and another low between Greenland and Newfoundland. Depicted as an anomaly with respect to the total climatology, the conditional climatology (c) reveals an East-West SLP dipole centred over the North Sea. The location of the SLP minimum is in good agreement with the surge-favorable conditions reported in the literature.

Figure. 3.12 shows SLP composites and their anomalies with respect to the full seasonal climatology in Fig. 3.11a for days satisfying the precipitation criterion for 1-day, 10-day and 20-day precipitation events. For the 1-day event, the dominant feature is a negative SLP anomaly centred over Denmark. For the multi-day events, a weaker negative SLP anomaly is featured but is positioned further to the south east, as well as a positive anomaly to the west of France. Note that the reference date (Fig. 2.2) is used for these composites, meaning that the rainfall has occurred over the *n*-days preceding the synoptic situation shown. For all three precipitation summation periods shown, the SLP anomaly configuration favours Northerly or Northwesterly wind flow over the North Sea.

Figure 3.13 displays composites satisfying both the surge and precipitation extreme criteria and their anomalies with respect to the full seasonal climatology. The anomaly dipole structures are heavily influenced by the requirement to fulfil the NNW wind criterion. The dipole pattern is similar to that for the climatology of days satisfying the wind conditions alone (Fig. 3.11c) but the amplitude is stronger. There is much more ridging evident over the Atlantic, compared to the composites conditioned on precipitation only (Fig. 3.12).

Figure 3.14 shows the anomaly composite for the joint event for $n = 20$ as a temporal sequence from 1 day before the reference date to 19 days before the reference date. Over this period, two synoptic regions of anomolous low pressure pass central Europe in the composite (see labels A and B in Fig. 3.14). A single event contributing to this composite is singled out for comparison in Fig. 3.15. There are approximately 6 synoptic low pressure systems (labels A to F) and their troughs that contribute to precipitation over the Rhine basin. Clearly a succession of low pressure systems contribute to the precipitation maximum. A notable feature is the strong ridging over the east Atlantic that causes low F to move south over Europe and brings Northerly winds over the UK and the North Sea. This feature — the rotation of a synoptic region of low pressure about a strong ridge, is also present in the composite (Fig. 3.14).

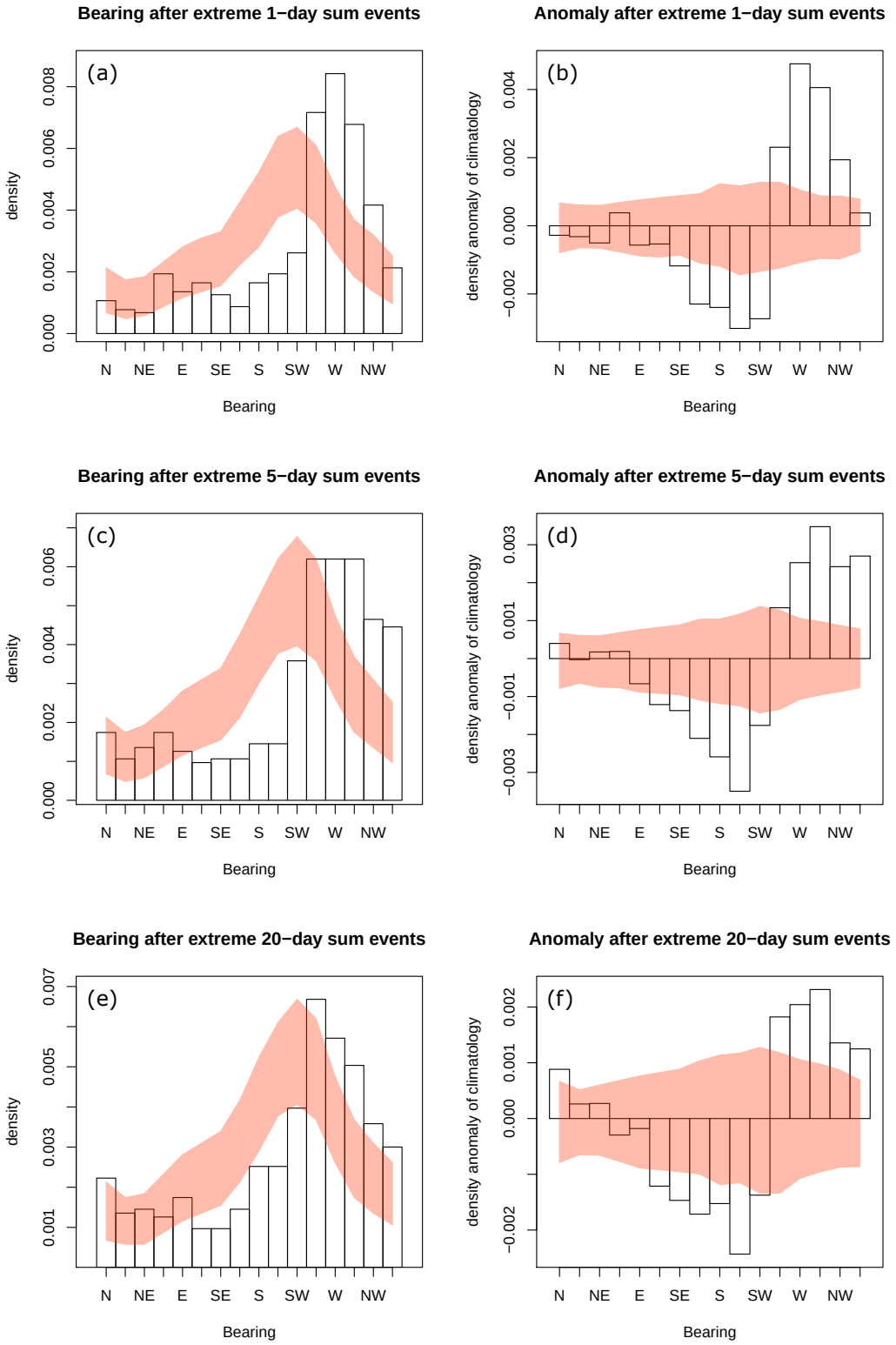

Figure 3.2: Wind directions following extreme (bars) and random samples (95% density range, shaded) of n-day precipitation sums (left) and their anomaly (right) with reference to the climatology.

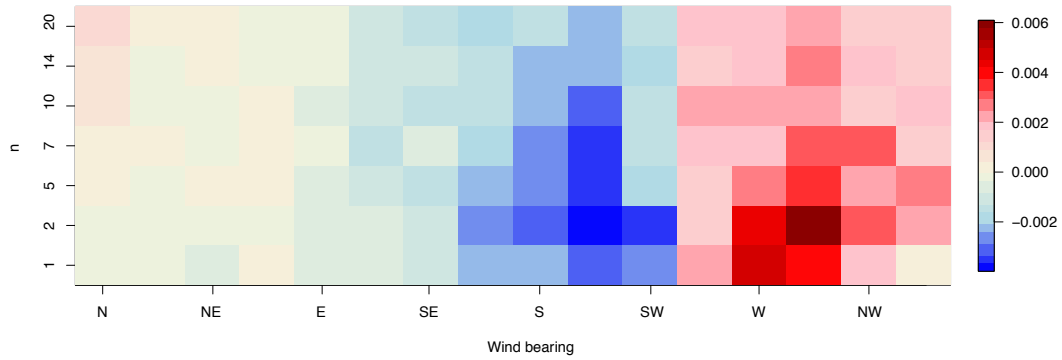

Figure 3.3: Anomaly in probability density for wind direction as a function of angle (in bins of 22.5° centred on traditional bearings) and the n – day summation interval, following extreme precipitation events.

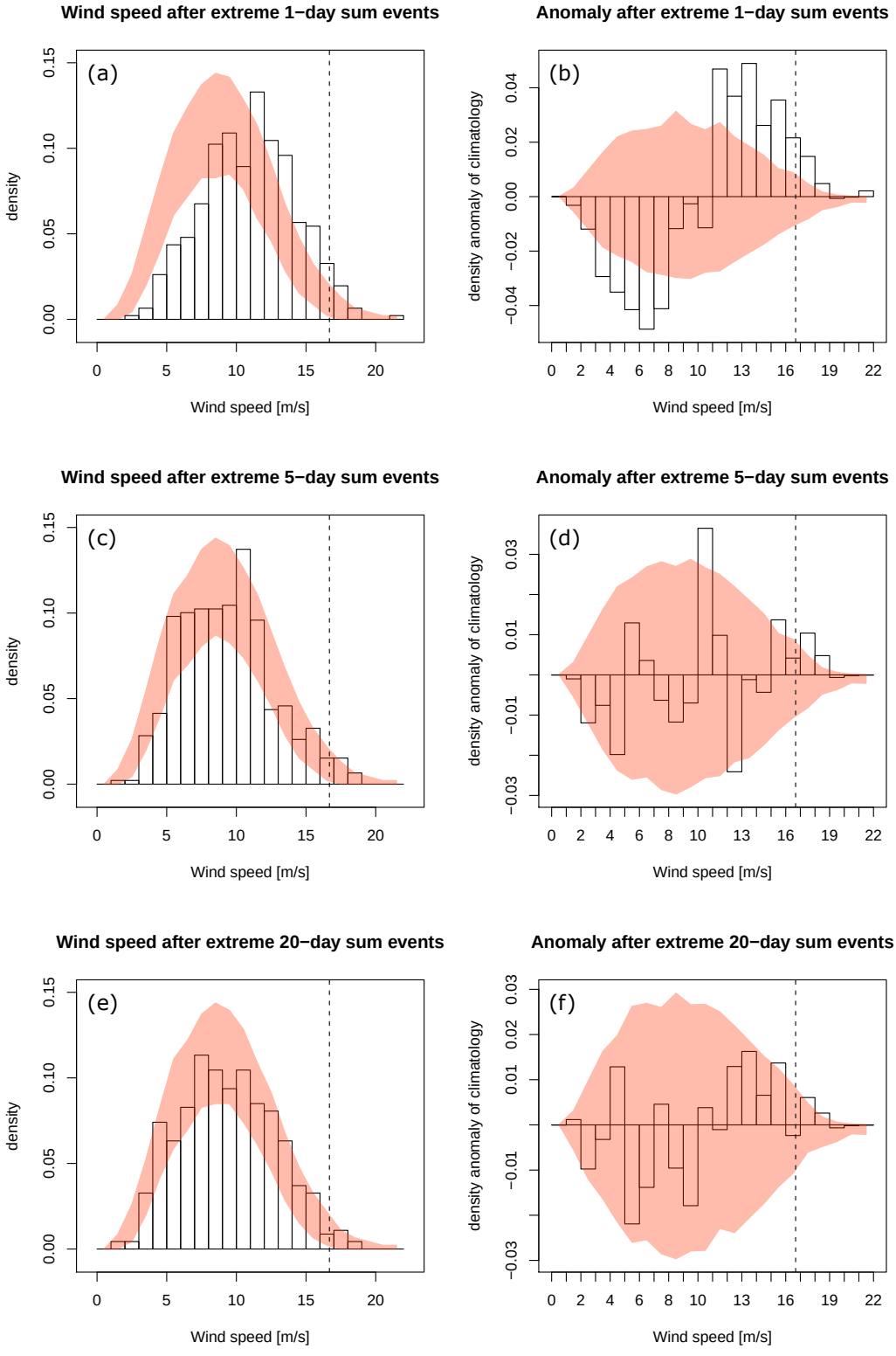

Figure 3.4: Wind speed following extreme n-day precipitation sums (left) and their anomaly with reference to the climatology (right). The $q_{0.99}$ threshold for wind speed is marked with a dashed line.

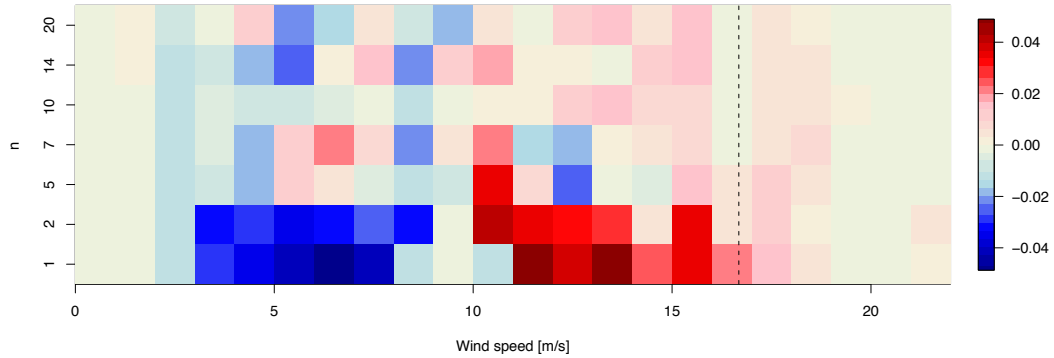

Figure 3.5: Anomaly in probability density for wind speed as a function of speed (in bins of 1 ms^{-1}) and the n−day summation interval, following extreme precipitation events. The $q_{0.99}$ for wind speed is marked by a dashed line.

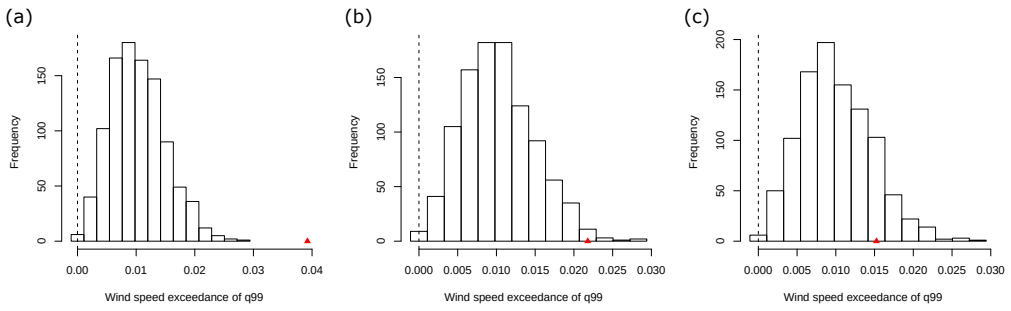

Figure 3.6: Exceedance of the climatological $q^{w}_{0.99}$ for the wind speed following extreme (a) 1-day (b) 5-day and (c) 20-day precipitation sums (red triangle) and 1000 random samples of the same size (bars). The vertical dashed lines enclose 99% of the 1000 samples.

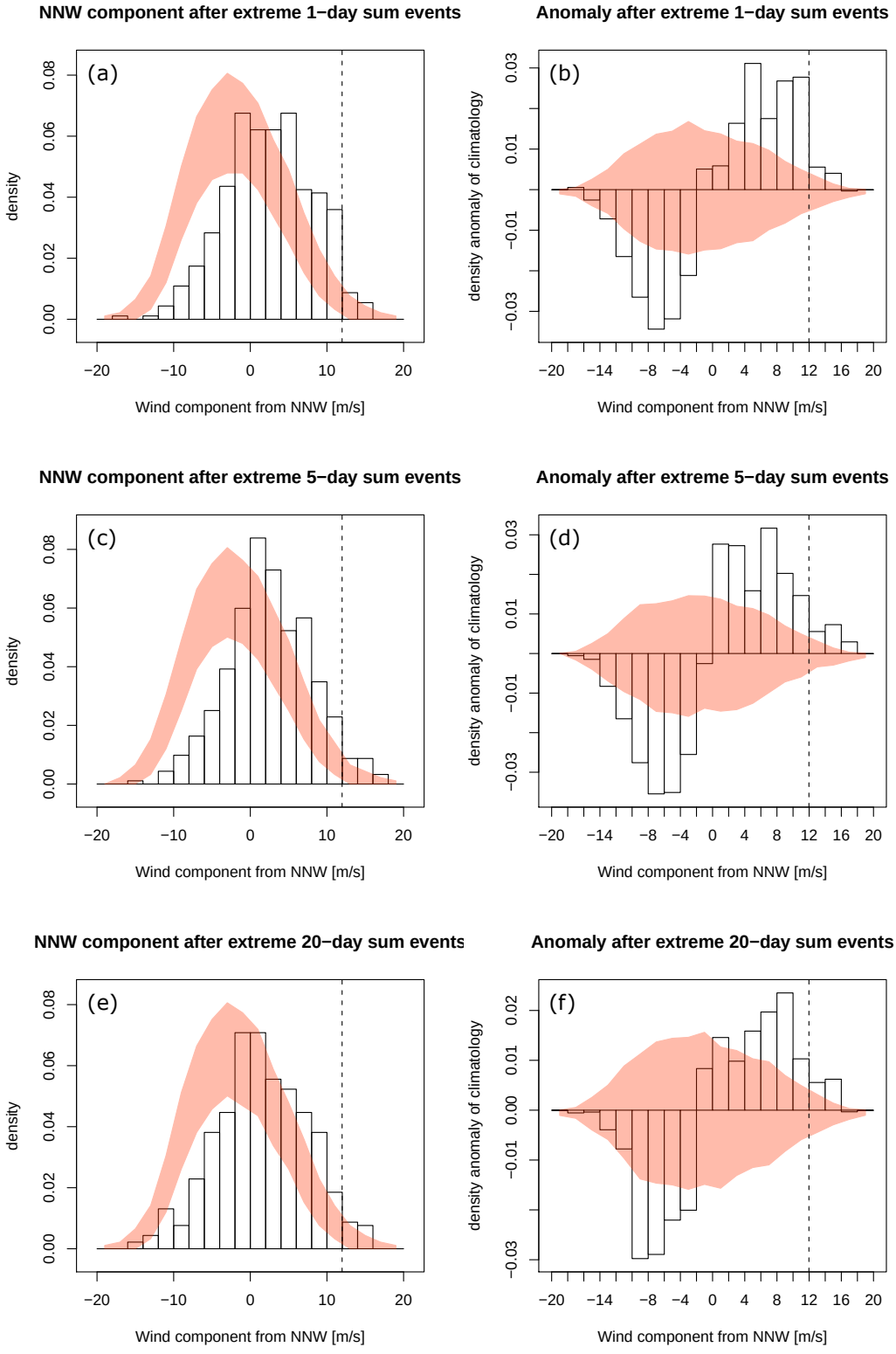

Figure 3.7: NNW wind component following extreme n-day precipitation sums (left) and their anomaly with reference to the climatology (right). The $q^{w}_{0.99}$ threshold is marked with a dashed line.

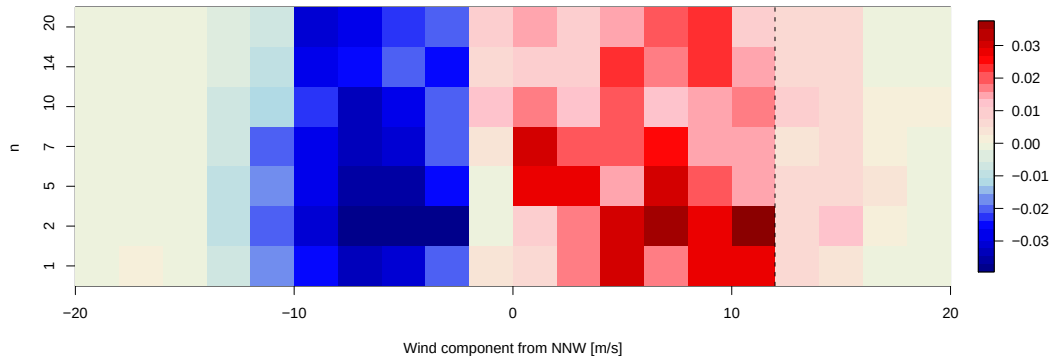

Figure 3.8: Anomaly in probability density for NNW wind component as a function of speed (in bins of 1 ms^{-1}) and the $n-$day summation interval, following extreme precipitation events. The $q^{w}_{0.99}$ threshold is marked with a dashed line.

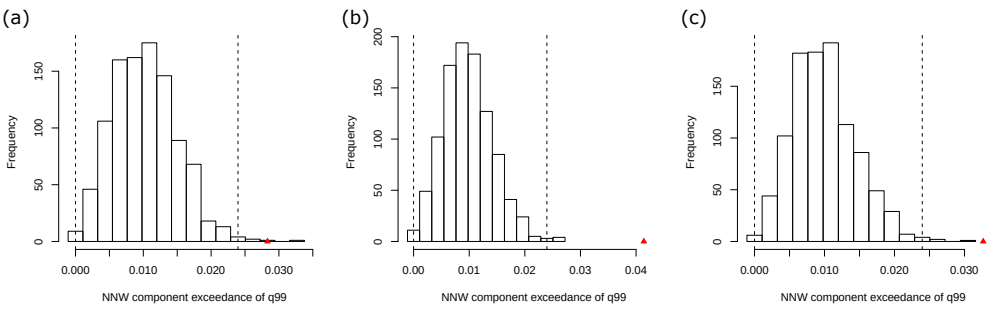

Figure 3.9: Exceedance of the climatological $q^{w}_{0.99}$ for the NNW wind component following extreme (a) 1-day (b) 5-day and (c) 20-day precipitation sums (red triangle) and 1000 random samples of the same size (bars). The vertical dashed lines enclose 99% of the 1000 samples.

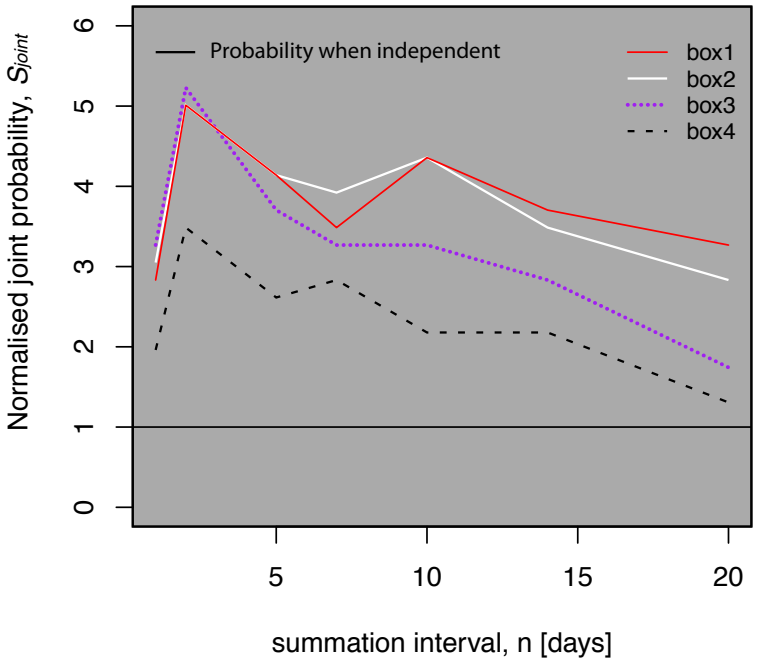

Figure 3.10: Summary of effect of changing North Sea box dimensions on the normalised joint probability S_{joint} (exceedances of the climatological $q^{w}_{0.99}$) for NNW wind component. Configurations of the four North Sea boxes can be seen in Fig. 2.1 with the same colour coding.

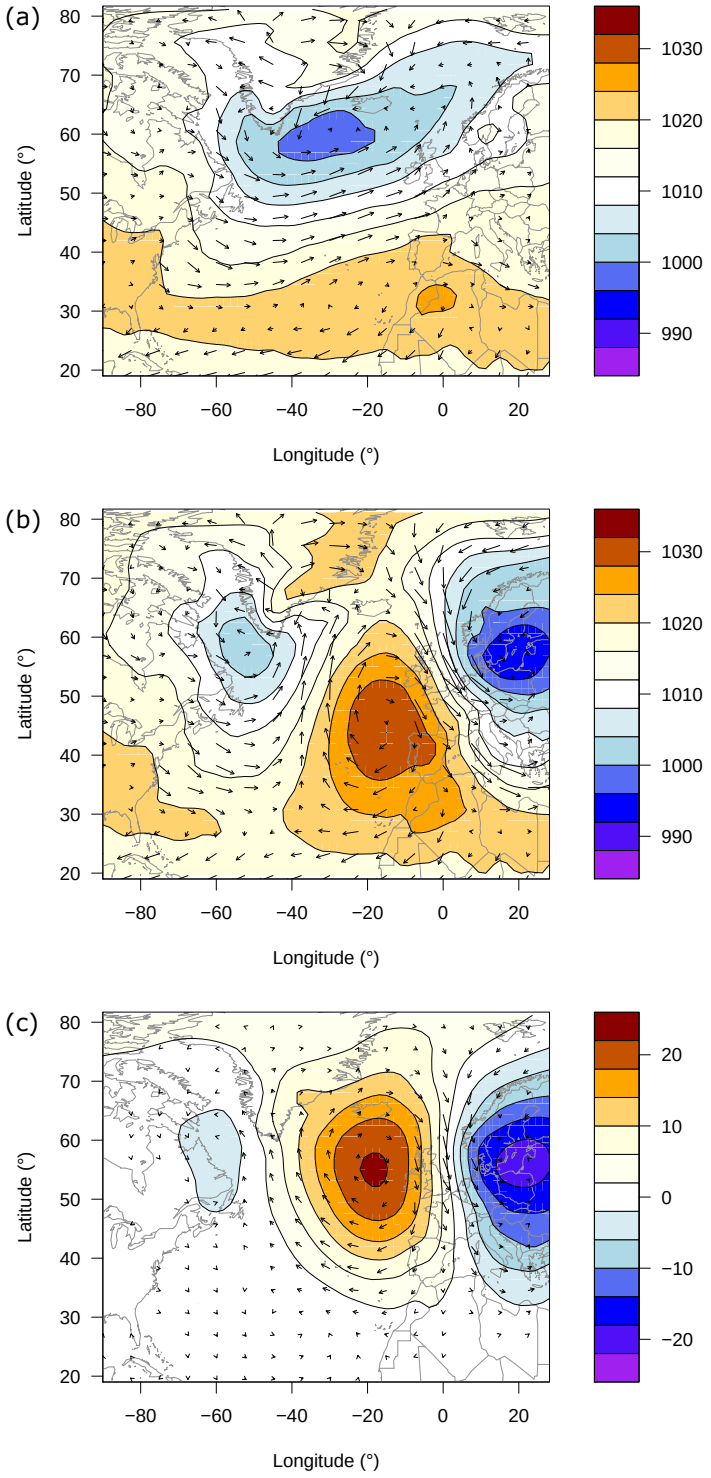

Figure 3.11: (a) SLP climatology in hPa (45900 entries) for DJF, (b) climatology conditioned on wind criterion (459 entries), (c) anomaly of conditional climatology with respect to full climatology (b − a).

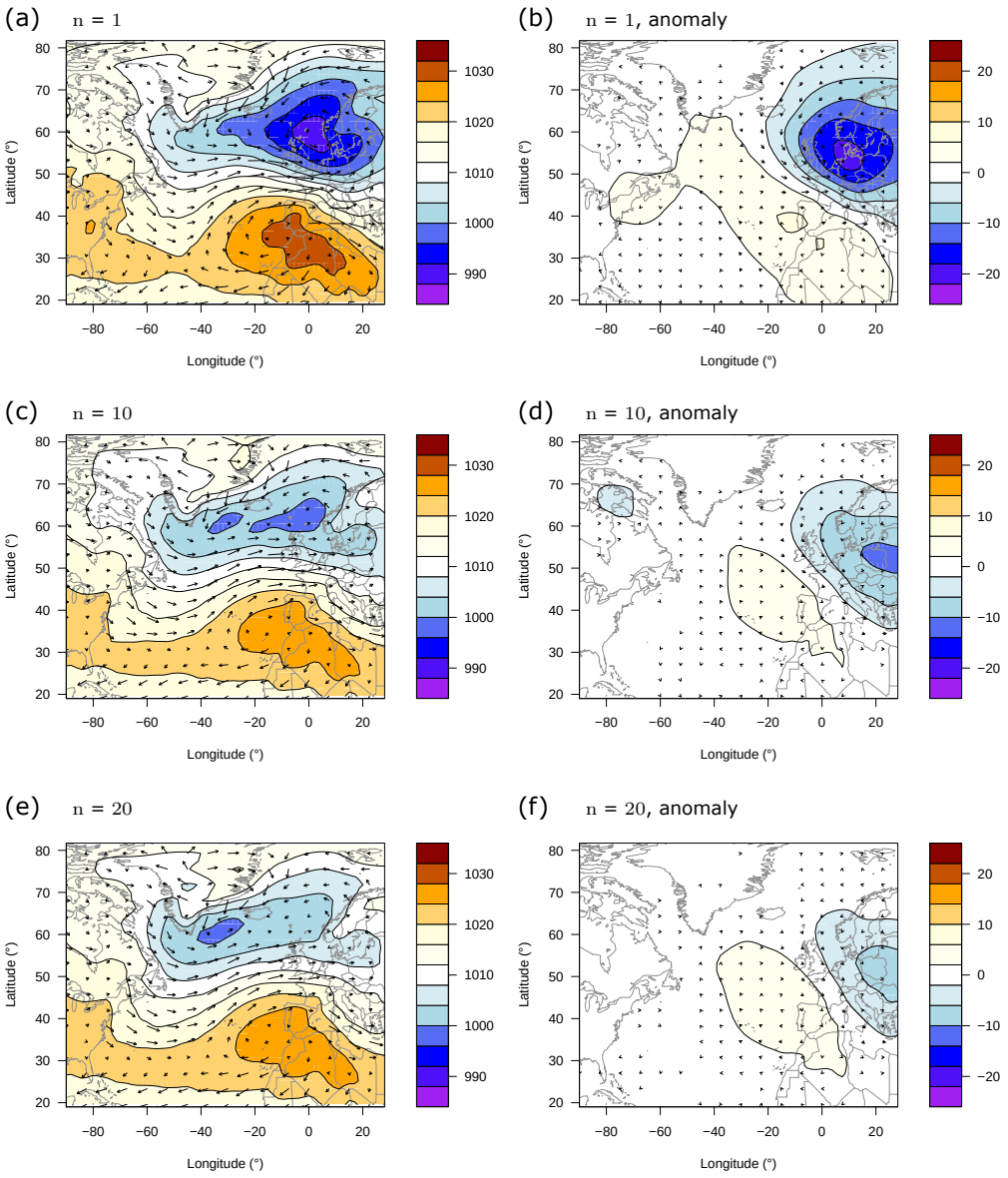

Figure 3.12: SLP climatology in hPa conditioned on 1-day (a-b), 10-day (c-d) and 20-day (e-f) precipitation extremes. Each panel contains 459 entries. Left hand column contains conditional SLP climatologies, right hand column contains the anomaly of the conditional climatology with respect to the full climatology in Fig. (3.11a).

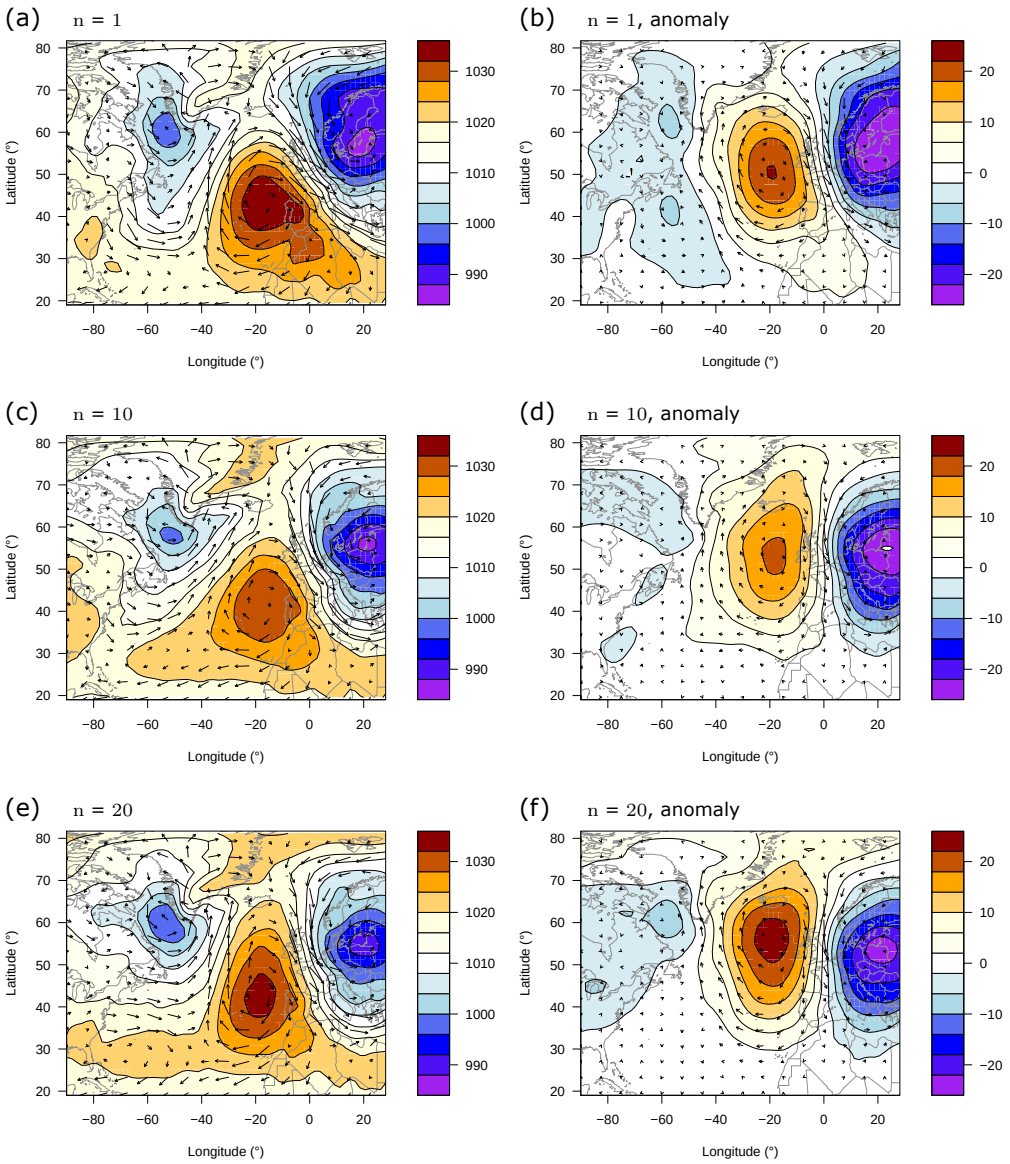

Figure 3.13: SLP climatology in hPa conditioned on both wind and precipitation extremes following 1-day (a-b), 10-day (c-d) and 20-day (e-f) precipitation sums. Each panel contains on the order of 20 entries. Left hand column contains conditional SLP climatologies, right hand column contains the anomaly of the conditional climatology with respect to the full climatology in Fig. (3.11a).

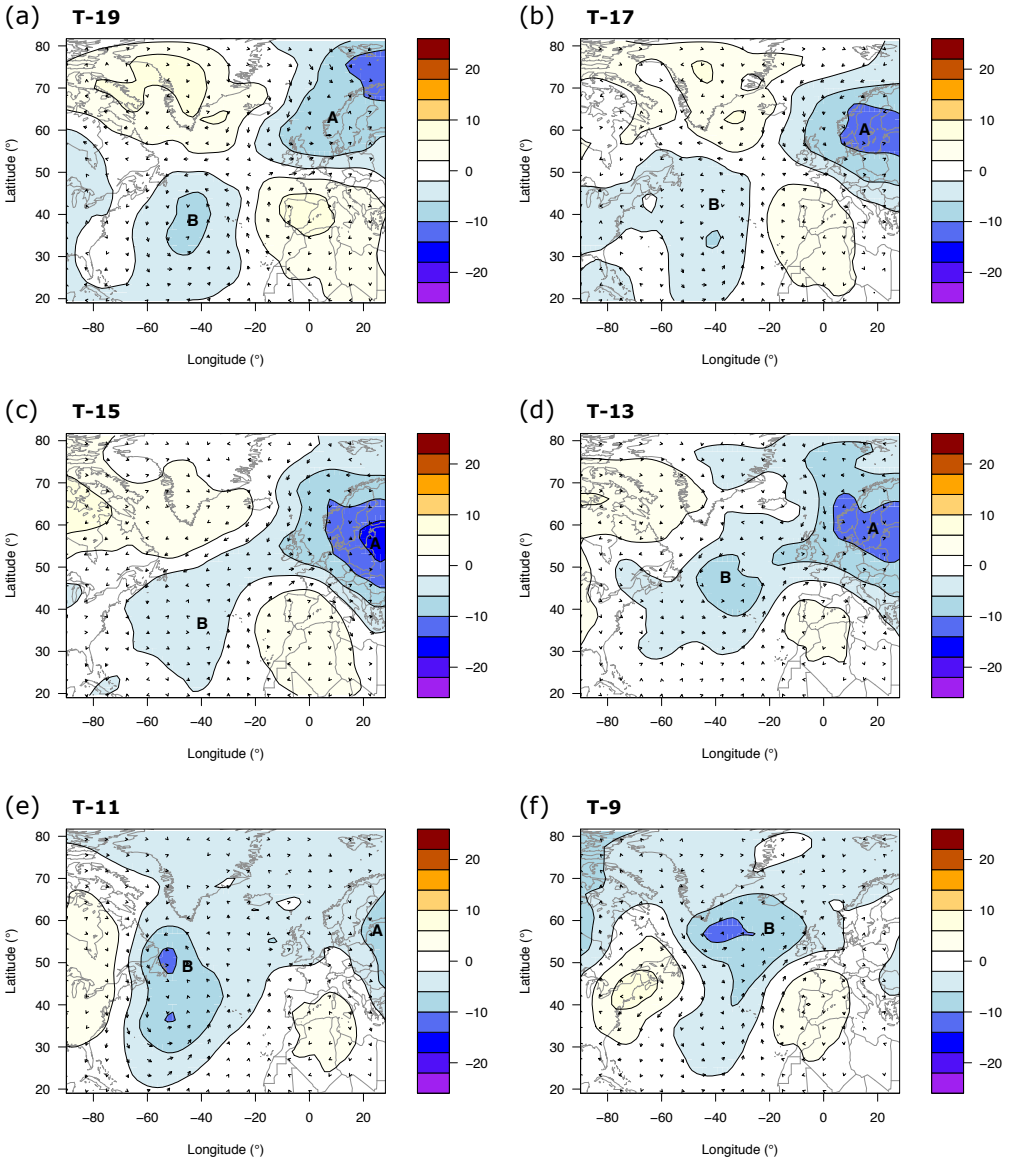

Figure 3.14: Evolution of the composite SLP anomaly in hPa, with respect to the full climatology in Fig. (3.11a). The composite contains the 15 events that satisfy the joint extreme conditions at $t = T - 0$. Labels A and B indicate 2 synoptic regions of anomalously low SLP that influence the Rhine region.

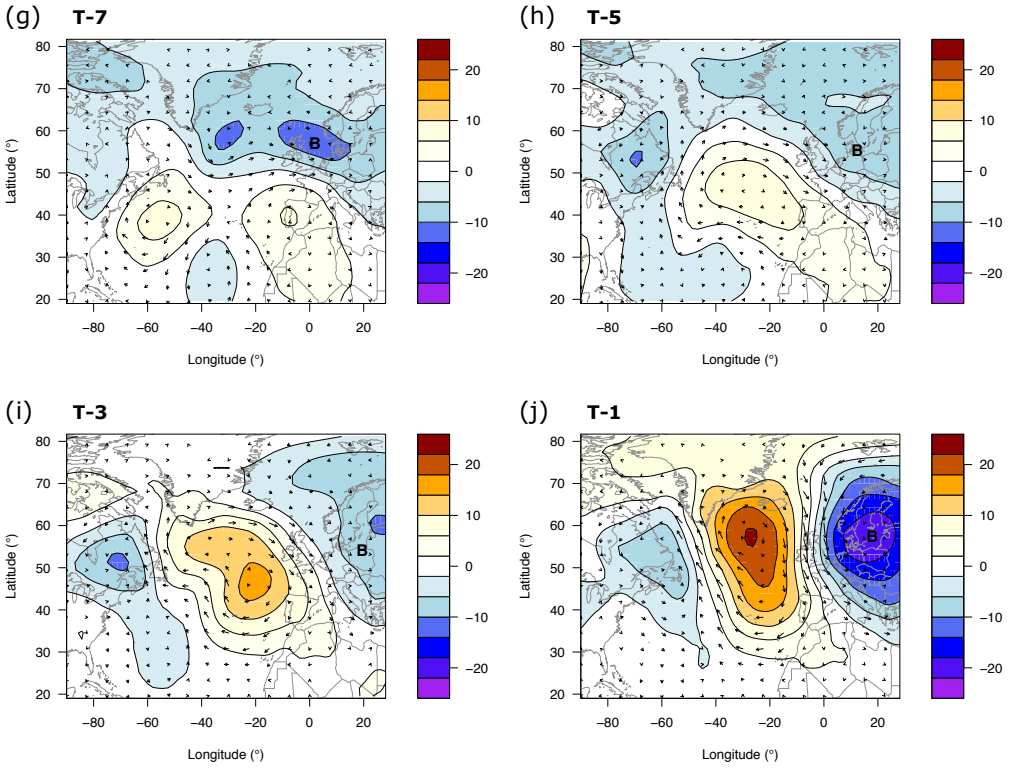

Figure 3.14: continued

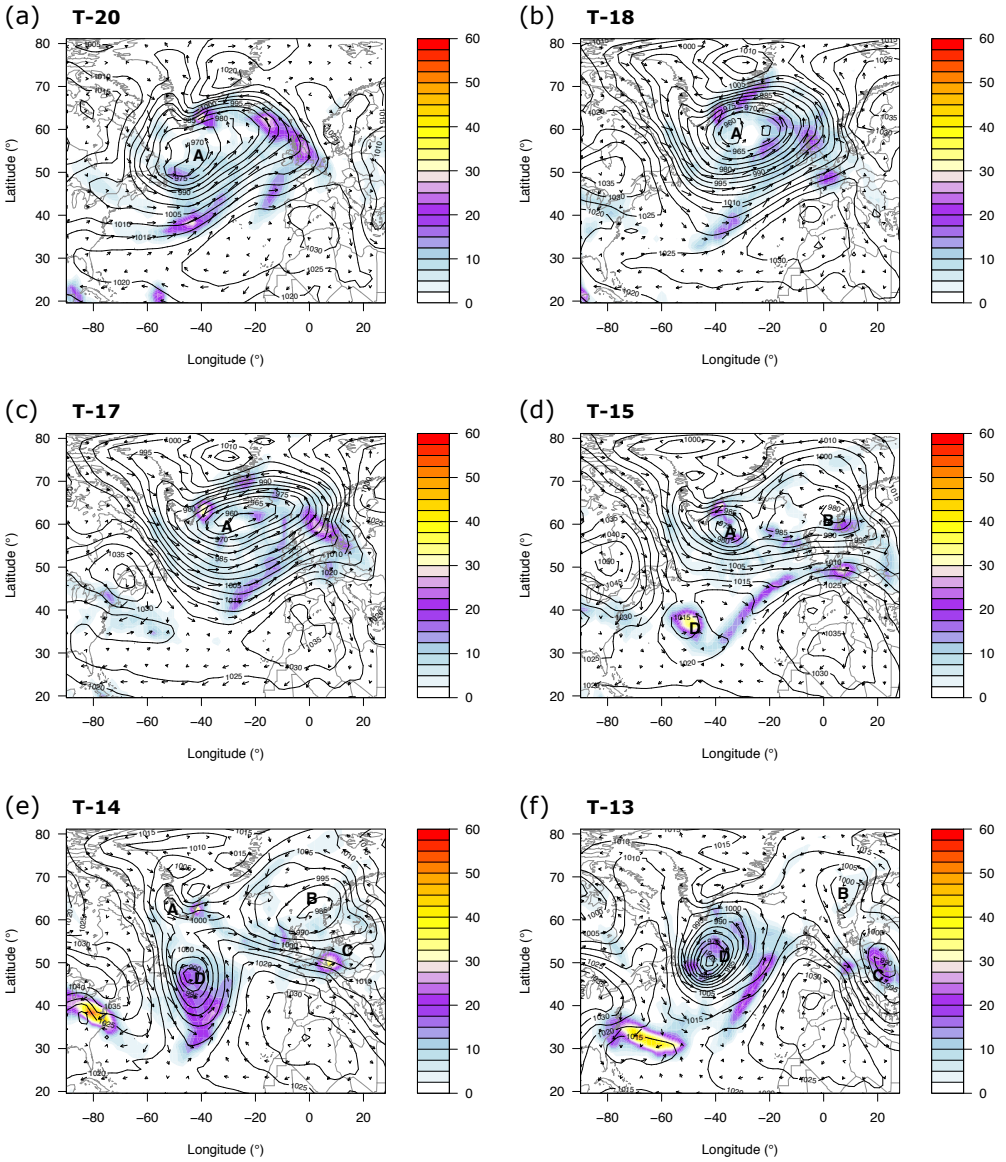

Figure 3.15: Evolution of synoptic situation for a single event that satisfied the joint extreme condition at t = T−0. The SLP field (12 UTC) in hPa is contoured, precipitation in mm/24h is shaded, daily average wind vectors are superimposed. Labels A to F indicate 6 synoptic regions of low SLP that influence the Rhine region.

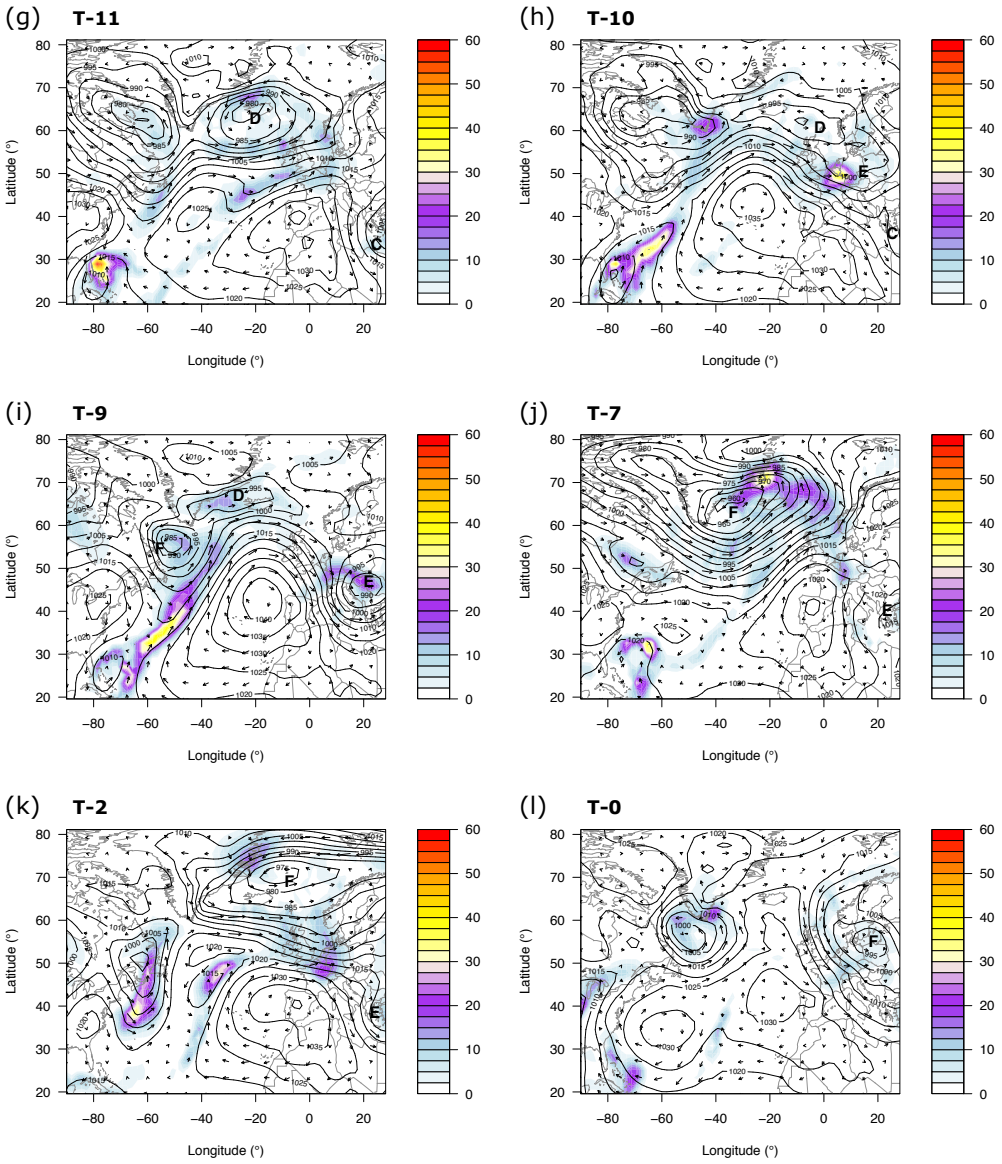

Figure 3.15: continued

4 Conclusions

4.1 Summary

After extreme rain over the Rhine basin, we find that the probability distribution of North Sea wind strength and direction shows significant departures from climatology. Wind directions in the West to North West quarter are favoured following both single and multi-day precipitation events, whilst the climatological mode direction, SW, is less favoured.

Sampled over all directions, wind speeds are significantly larger than climatology only following extreme precipitation events of short duration. The magnitude of the wind projected in the NNW direction, however, increases over climatological values also for multiday events, including extremes ($w_1 > q^w_{0.99}$). The exceedance of the $q^w_{0.99}$ threshold was shown to be outside of the range that can be expected from sampling error. These changes therefore suggest that the probability of a surge conditioned on preceding heavy precipitation is indeed larger than when independence is assumed.

The probability of a NNW wind extreme conditioned on a preceding 20-day rain extreme (as seen in Fig. 3.10) is over 3 times greater than for the unconditioned case (using Box 1 of Fig. 2.1 for the wind conditions). Although this increase is significant, it is still quite small — approximately 97% of surge conditions occur without a preceding 20-day precipitation extreme. Fig. 4.1 illustrates the results schematically with Venn diagrams. The area of overlap between the set w^*_1 of wind extremes and the set r^*_{20} of precipitation extremes increases more than 3-fold between panel (a) and (b), but the joint events are still a tiny fraction of the two individual sets.

To place these results in context with those of Van den Brink et al. (2005), we produced our own version (Fig. 4.2) of their Fig. 6b (see Fig. 1.1). We plot 20-day precipitation sums instead of Rhine discharge, and North Sea NNW wind component instead of the Sea Level at Hoek van Holland and, for clarity, display density contours rather than a scatter plot. Just as for Fig. 6b of Van den Brink et al. (2005), there is no correlation to be seen between the two variables (black contours, Fig. 4.2).

In addition, we simulated a distribution where we know that the wind and precipitation variables are independent (grey contours). It is made by replacing the actual wind values, following each 20-day precipitation sum, with wind values selected randomly from all days. A comparison between the two distributions (black and grey) allows the way in which the actual distribution departs from the assumptions of independence to be visualised. Shaded black (grey) regions indicate where the actual distribution's density is larger (smaller) than that of the independent probability distribution for a given NNW wind component. Although we have only investigated soft extremes, it is evident that the departures from the independent distribution are greatest in the top right hand segment of the figure, i.e. in the tail of the joint distribution. The shift of the PDF for the conditional samples with respect to the climatology (see Fig. 3.7c) can also be gleaned from this figure, by noting the pattern of grey and black areas in the regions exceeding the $q_{0.99}$ thresholds (dashed lines).

Finally, inspection of the SLP composites satisfying the joint conditions for wind and rain extremes shows an intuitive sequence where, for a 20-day extreme precipitation sum, rain is accumulated from at least 2 synoptic systems and the North Sea surge conditions are generated at the rear of the final system as it passes across southern

Scandinavia.

4.2 Recommendations

The joint probability was found to be sensitive to the North Sea box dimensions used for the wind conditions and to the length of the precipitation sum used as a proxy for discharge. It would be instructive and straight forward to test the following parameters in an extended sensitivity analysis:

- Rhine basin box dimensions
- Lag between the precipitation reference date and the wind assessment
- Position of reference date in precipitation block
- Start date and number of years included in the climatology
- Season
- Axis of projection for winds
- Duration of wind condition
- Quantile defining extreme discharge event
- Quantile defining extreme surge event.

Whilst this simple set up is useful for preliminary investigations, there are several important factors which introduce further uncertainty and should be taken into account in a more thorough investigation using sophisticated surge and discharge models. These are, for example, the contribution to discharge of rapid snow melt, the possibility of dam breeches upstream, the river basin configuration and tides. Changes to the joint probability of extreme surge and discharge events in the future are likely from sea-level rise, increases in storm frequency or intensity, and earlier and potentially more rapid snow melt.

We particularly recommend a comparison of the present results for the current climate with the output of coupled surge-discharge models when driven by the same global ensemble (containing the same synoptic systems).

A major question remaining is how these results extend to more extreme events with multiple-year return periods.

Acknowledgments

This study is part of the project *Future Weather* and was carried out in the framework of the Dutch National Research Programme Knowledge for Climate (www.knowledgeforclimate.org). This research programme is co-financed by the Ministry of Infrastructure and the Environment.

The authors wish to acknowledge Deltares for their interest, discussions and suggestions for future work.

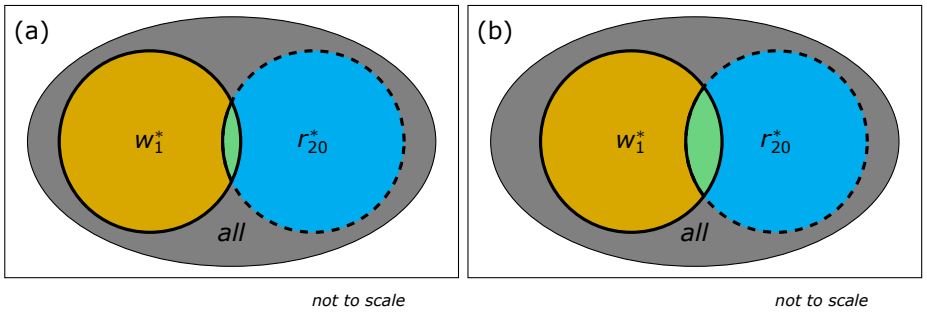

Figure 4.1: Venn diagrams showing schematically the set of wind extremes (w_1^*, yellow) and 20-day precipitation extremes (r_{20}^*, blue) as subsets of the total data available (grey) and their overlap (green). By construction, both the w_{1*} and r_{20}^* subsets are 1% of all days. If the wind extremes are independent of the precipitation extremes, the probability of the joint event (green overlap) is $P(w_{1*})P(r_{20}^*)$ = 0.01% of the total number of days, or equivalently, 1% of wind extremes occur by chance within the subset of precipitation extremes (a). However, ESSENCE data shows the percentage of joint events (green overlap) to be 2-4 times larger (b), considering 20-day precipitation events. There are still however a large proportion of wind extremes (b, yellow) that do not overlap with the set of extreme precipitation events.

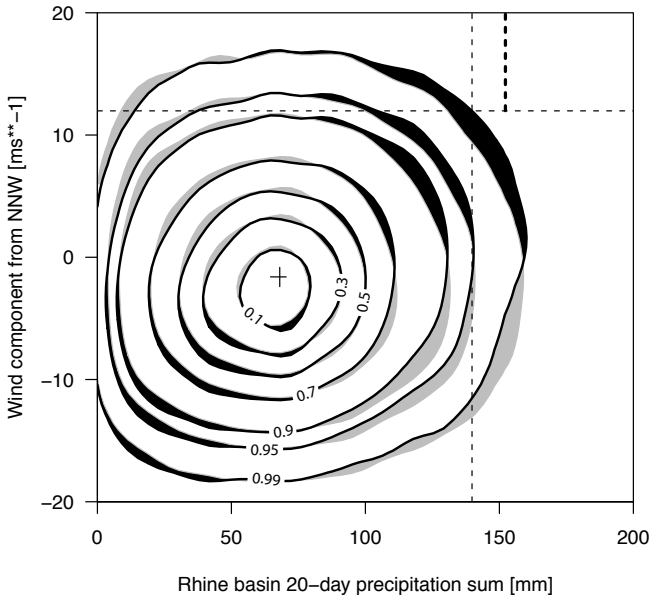

Figure 4.2: Data density (kernel density estimation) for Rhine basin 20-day precipitation sums against the North Sea NNW wind component evaluated on the last of the 20-days. Labels indicate the proportion of the data cloud enclosed by the contours. Black contours are for the pure results from the ESSENCE data set. Grey contours show how the distribution would look if the two variables were independent. Black (grey) shading is used where the true distribution's frequency density exceeds (undercuts) that of the independent distribution for the same NNW wind speed. Thin dashed lines show the 99% quantiles for each variable estimated from the pure data. The thick dashed line shows the 99% precipitation quantile of the sub group w_1^* satisfying $w_1 > q_{0.99}^w$. The cross marks the mean of the 2D distribution.

References

Katsman, C., Sterl, A., Beersma, J. J., van den Brink, H. W., Church, J. A., Hazeleger, W., Kopp, R. E., Kroon, D., Kwadijk, J., Lammersen, R., Lowe, J, Oppenheimer, M., Plag, H. P., Ridley, J., von Storch, H., Vaughan, D. G., Vellinga, P., Vermeersen, L. L. A., van de Wal, R. S. W. and Weisse, R., 2011. Exploring high-end scenarios for local sea level rise to develop flood protection strategies for a low-lying delta — the Netherlands as an example. *Climatic Change*, doi:10.1007/s10584-011-0037-5.

Kew, S. F., Selten, F. M., Lenderink, G., and Hazeleger, W., 2011. Robust assessment of future changes in extreme precipitation over the Rhine basin using a GCM. *Hydrol. Earth Syst. Sci.*, **15**:1157–1166.

Nakićenović, N., et al., 2000. Special Report on Emissions Scenarios. *A Special Report of Working Group III of the Intergovernmental Panel on Climate Change*, 599 pp., Cambridge Univ. Press, Cambridge, UK.

Sterl, A., van den Brink, H., de Vries, H., Haarsma, R., and van Meijgaard, E., 2009. An ensemble study of extreme storm surge related water levels in the North Sea in a changing climate. *Ocean Sci.*, **5**:369–378.

Sterl, A., Severijns, C., Dijkstra, H., Hazeleger, W., van Oldenborgh, G. J., van den Broeke, M., Burgers, G., van den Hurk, B., van Leeuwen, P. J., and van Velthoven, P., 2008. When can we expect extremely high surface temperatures? *Geophys. Res. Lett.*, **35**:L14703, doi:10.1029/2008GL034071.

Van den Brink, H. W., Können, G. P., Opsteegh, J. D., van Oldenborgh, G. J. and Burgers, G., 2004. Improving 10^4-year surge level estimates using data of the ECMWF seasonal prediction system. *Geophys. Res. Lett.*, **31**:L17210, doi:10.1029/2004GL020610.

Van den Brink, H. W., Können, G. P., Opsteegh, J. D., van Oldenborgh, G. J. and Burgers, G., 2005. Estimating return periods of extreme events from ECMWF seasonal forecast ensembles. *Int. J. Climatol.*, **25**:1345–1354.

A complete list of all KNMI-publications (1854 – present) can be found on our website

www.knmi.nl/knmi-library/knmipub_en.html

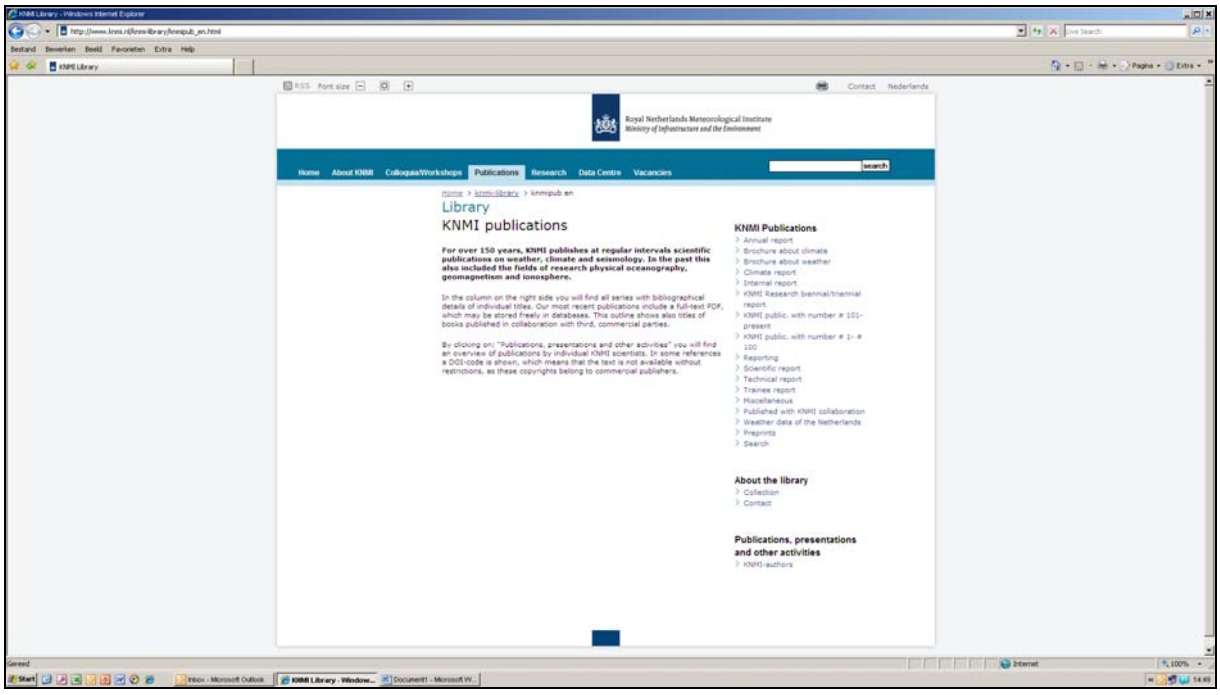

The most recent reports are available as a PDF on this site.